# -SUPPLEMENTARY MATERIAL-

# for

# Imaging of Transition Charge Densities Involving Carbon Core Excitations by All X-ray Sum-Frequency Generation

Daeheum Cho,[*,†,‡] Jérémy R. Rouxel,[¶,§] Markus Kowalewski,[‖] Jin Yong Lee,[*,‡] and Shaul Mukamel[*,†]

†*Department of Chemistry and Physics and Astronomy, University of California, Irvine, California 92697, United States*

‡*Department of Chemistry, Sungkyunkwan University, Suwon 16419, Korea*

¶*Laboratory of Ultrafast Spectroscopy, École Polytechnique Fédérale de Lausanne, CH-1015 Lausanne, Switzerland*

§*SwissFEL, Paul Scherrer Institut, 5232 Villigen PSI, Switzerland*

‖*Department of Physics, Stockholm University, AlbaNova University Center, 10691 Stockholm, Sweden*

E-mail: daeheumc@uci.edu; jinylee@skku.edu; smukamel@uci.edu

# Contents

# S1 MO shapes and Transition Charge Densities

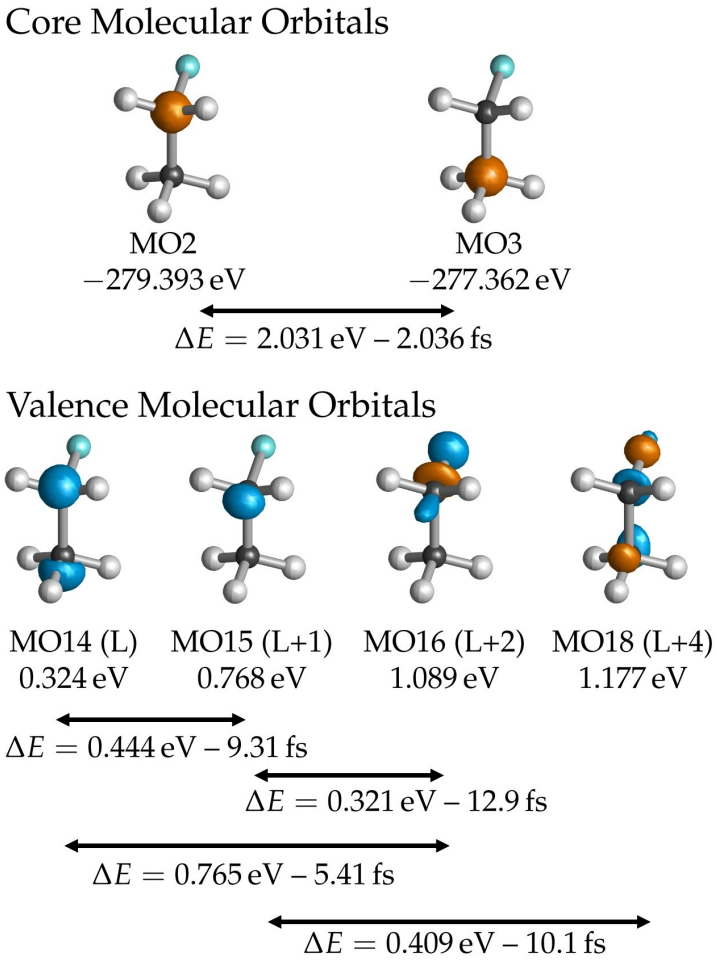


Figure S1: Core and valence MO shapes, energies, and energy differences. L: LUMO, L+$n$=LUMO+$n$.

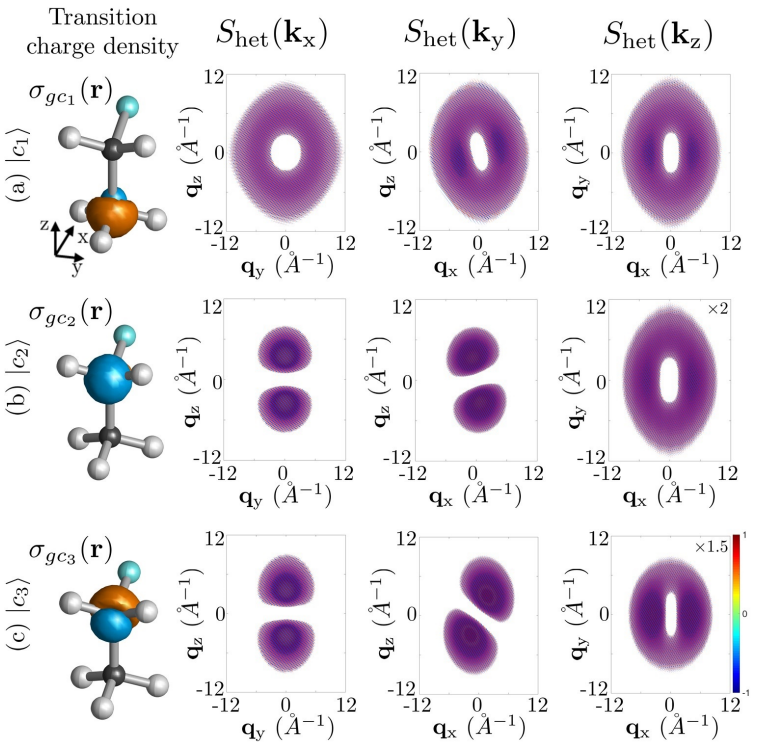


Figure S2: Static heterodyne imaging $S_{\mathrm{het}}$ of transition charge density $\sigma_{gc_i}$ responsible for (a) $|c_1\rangle$, (b) $|c_2\rangle$, and (c) $|c_3\rangle$ states calculated at the LR-REW-TDDFT/B3LYP/6-31+G* level (blue: electron, orange: hole density; isovalue of 0.01).

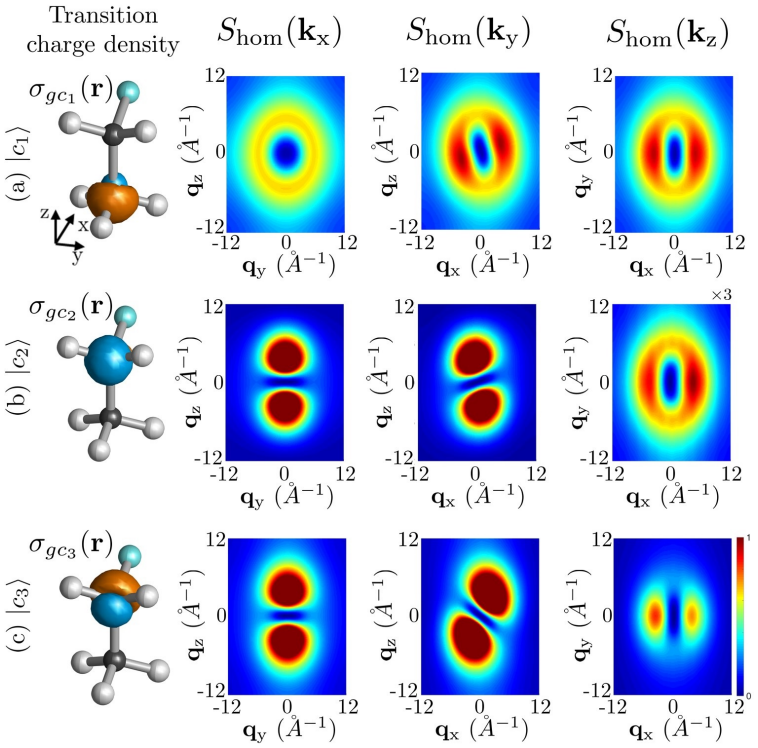


Figure S3: Static homodyne imaging $S_{\mathrm{hom}}$ of transition charge density $\sigma_{gc_i}$ responsible for (a) $|c_1\rangle$, (b) $|c_2\rangle$, and (c) $|c_3\rangle$ states calculated at the LR-REW-TDDFT/B3LYP/6-31+G* level (blue: electron, orange: hole density; isovalue of 0.01).

## S2 Attosecond Charge Migration due to Core Coherences and Femtosecond Charge Migration due to Valence Coherences

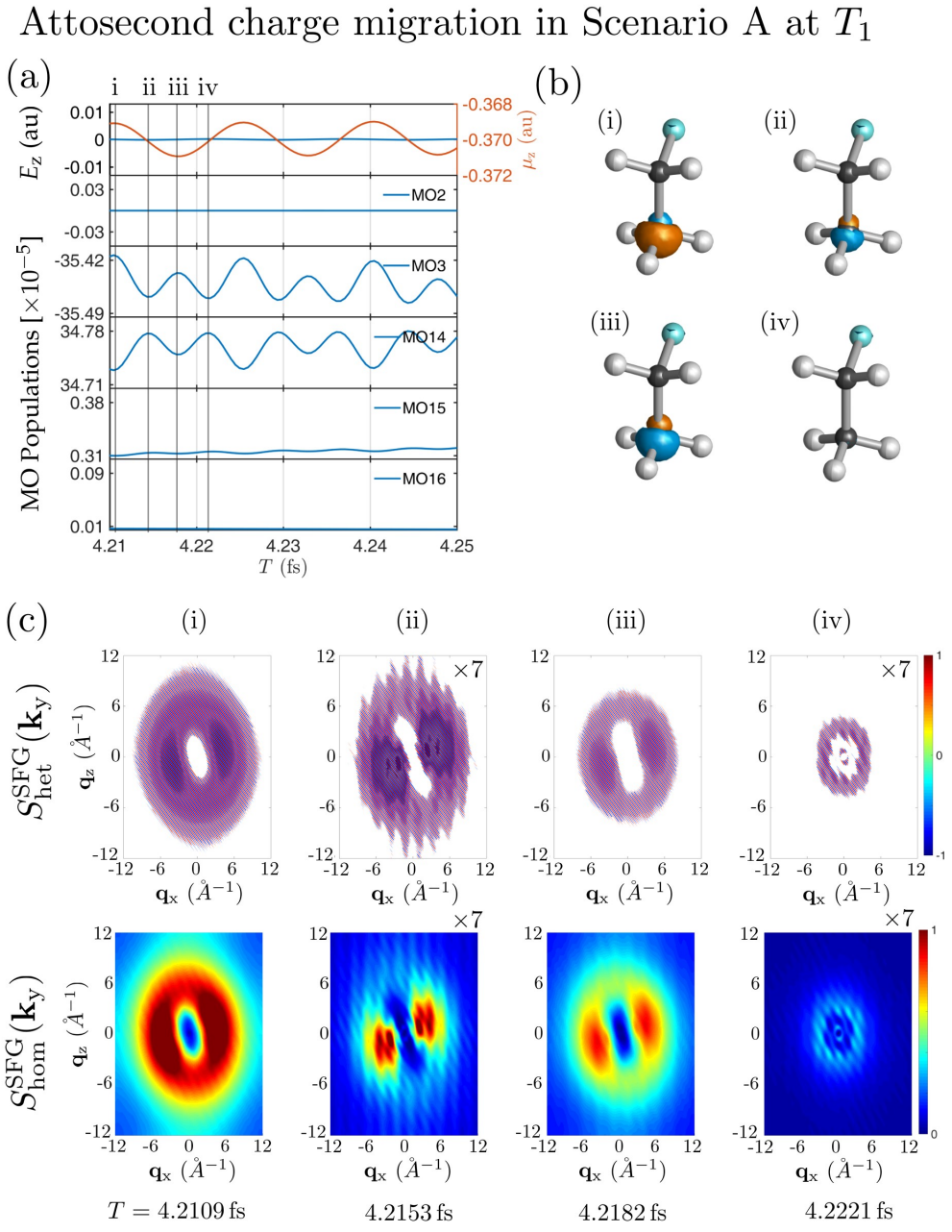


Figure S4: RT-TDDFT simulation of the electron-hole dynamics around $T_1$ following $|c_1\rangle$ excitation of fluoroethane. (a) Time-dependent $\mu_z$ and populations of dominant core and valence MOs. Key points are marked as i–iv. (b) Electron-hole densities. Blue: electron, orange: hole density. (c) Heterodyne and homodyne Diffraction signals.

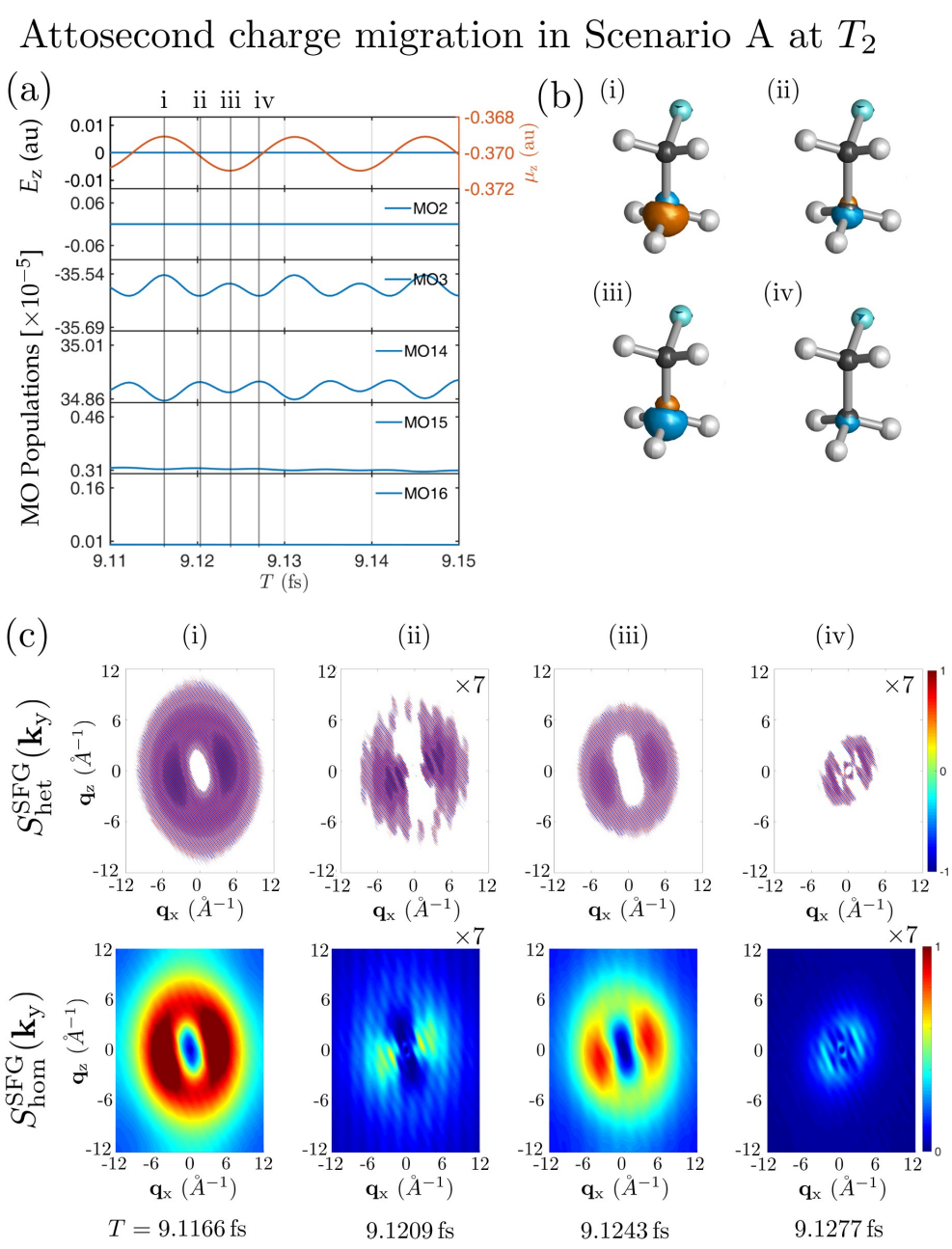


Figure S5: Same as Figure S4 but for Scenario A at $T_2$.

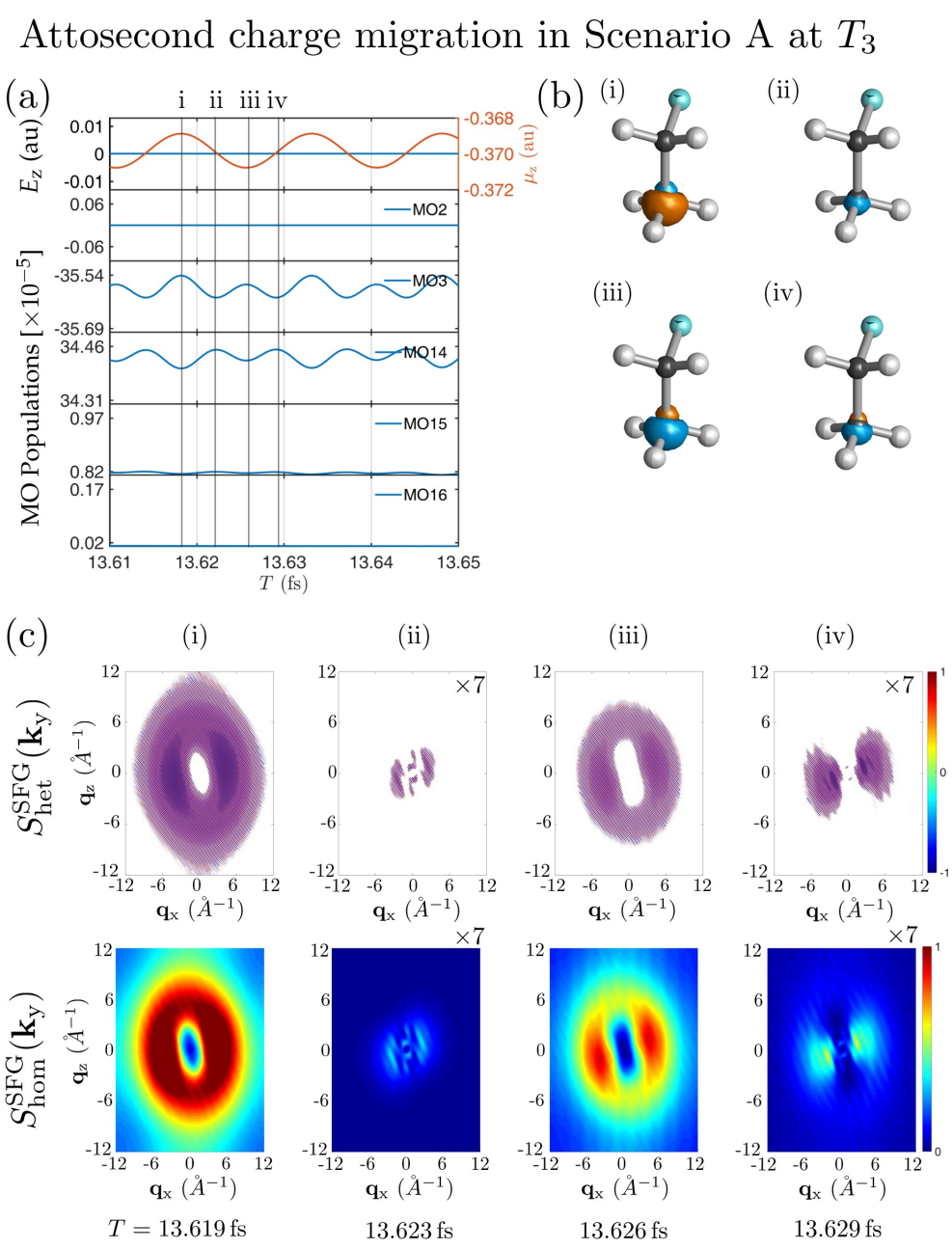


Figure S6: Same as Figure S4 but for Scenario A at $T_3$.

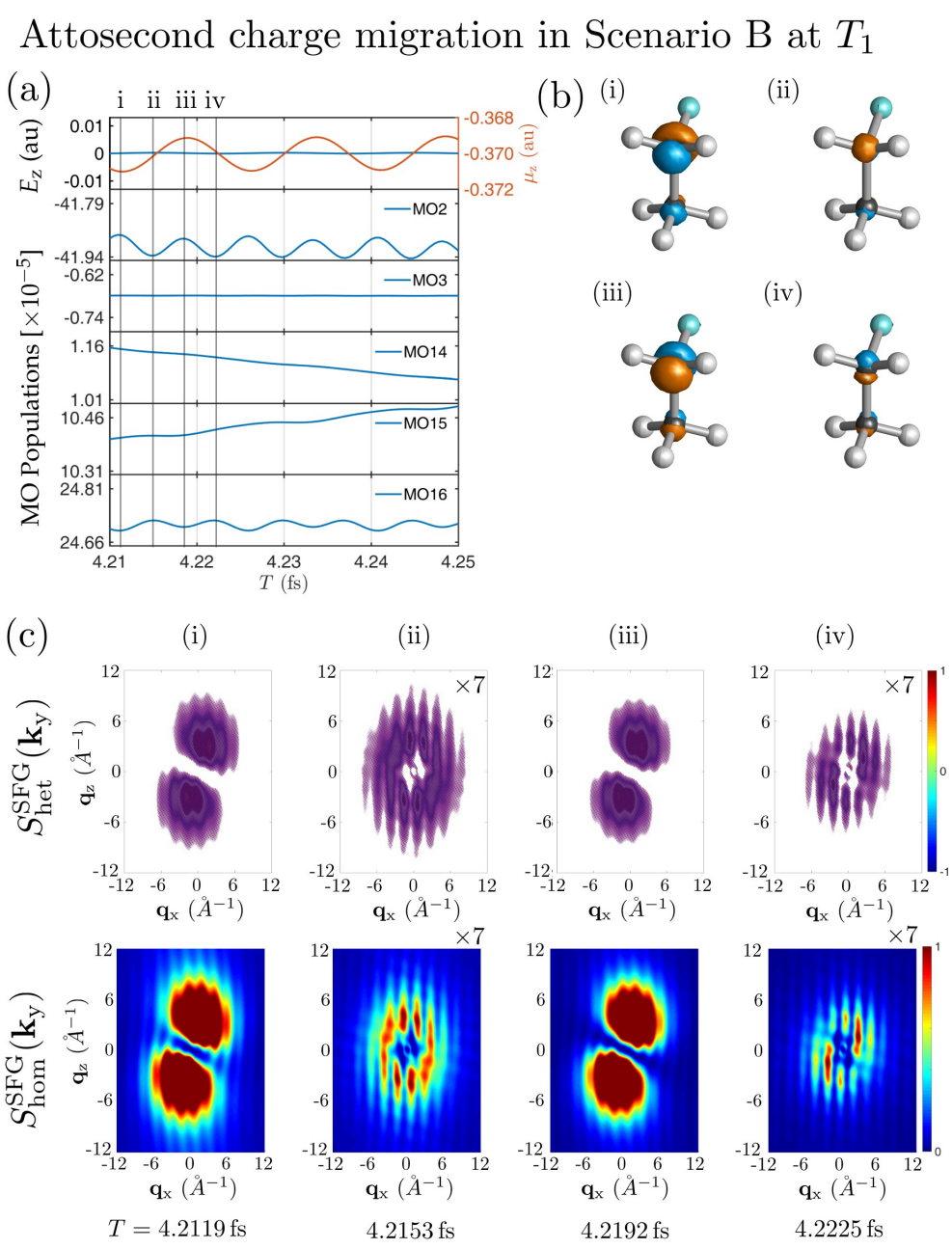


Figure S7: Same as Figure S4 but for Scenario B at $T_1$.

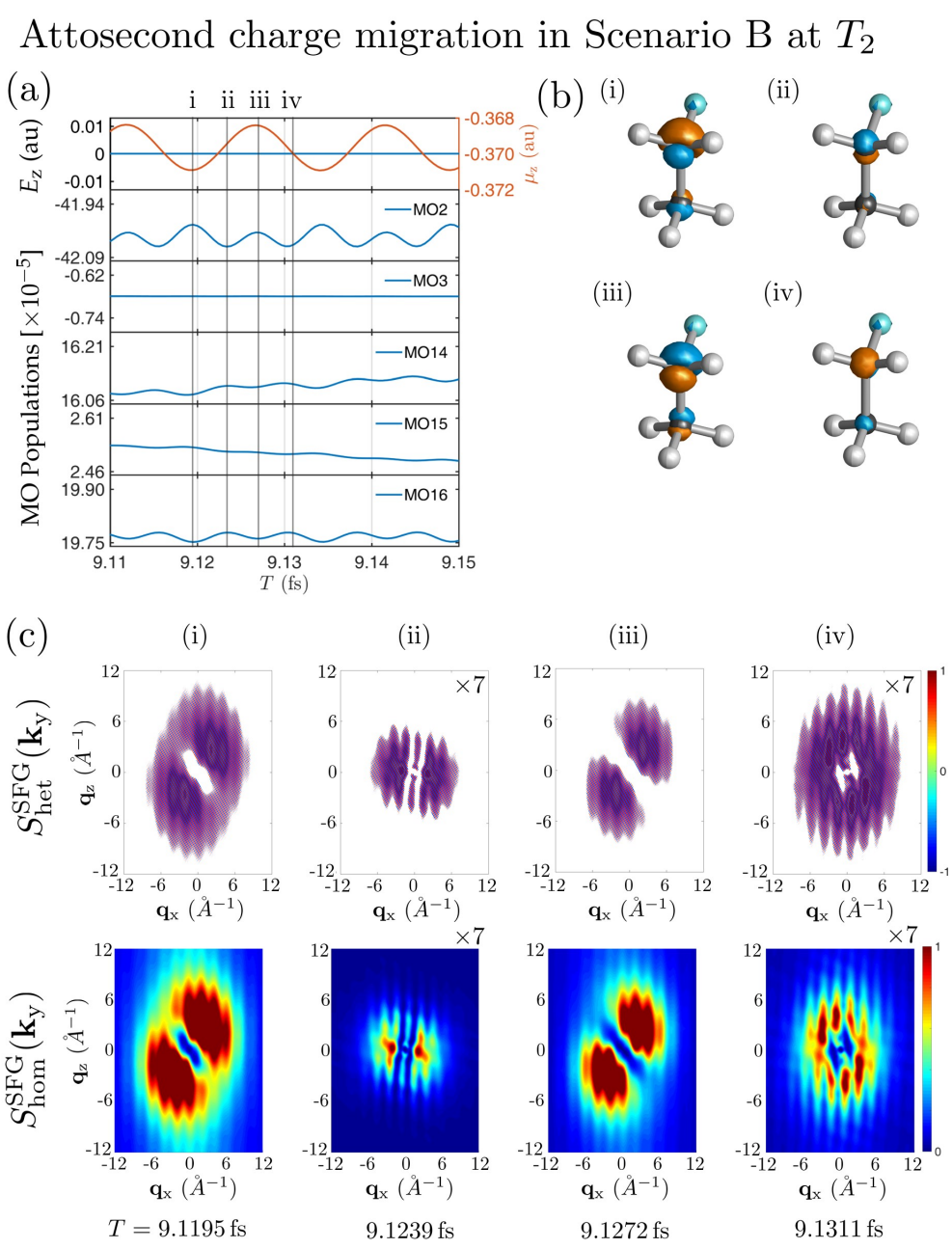


Figure S8: Same as Figure S4 but for Scenario B at $T_2$.

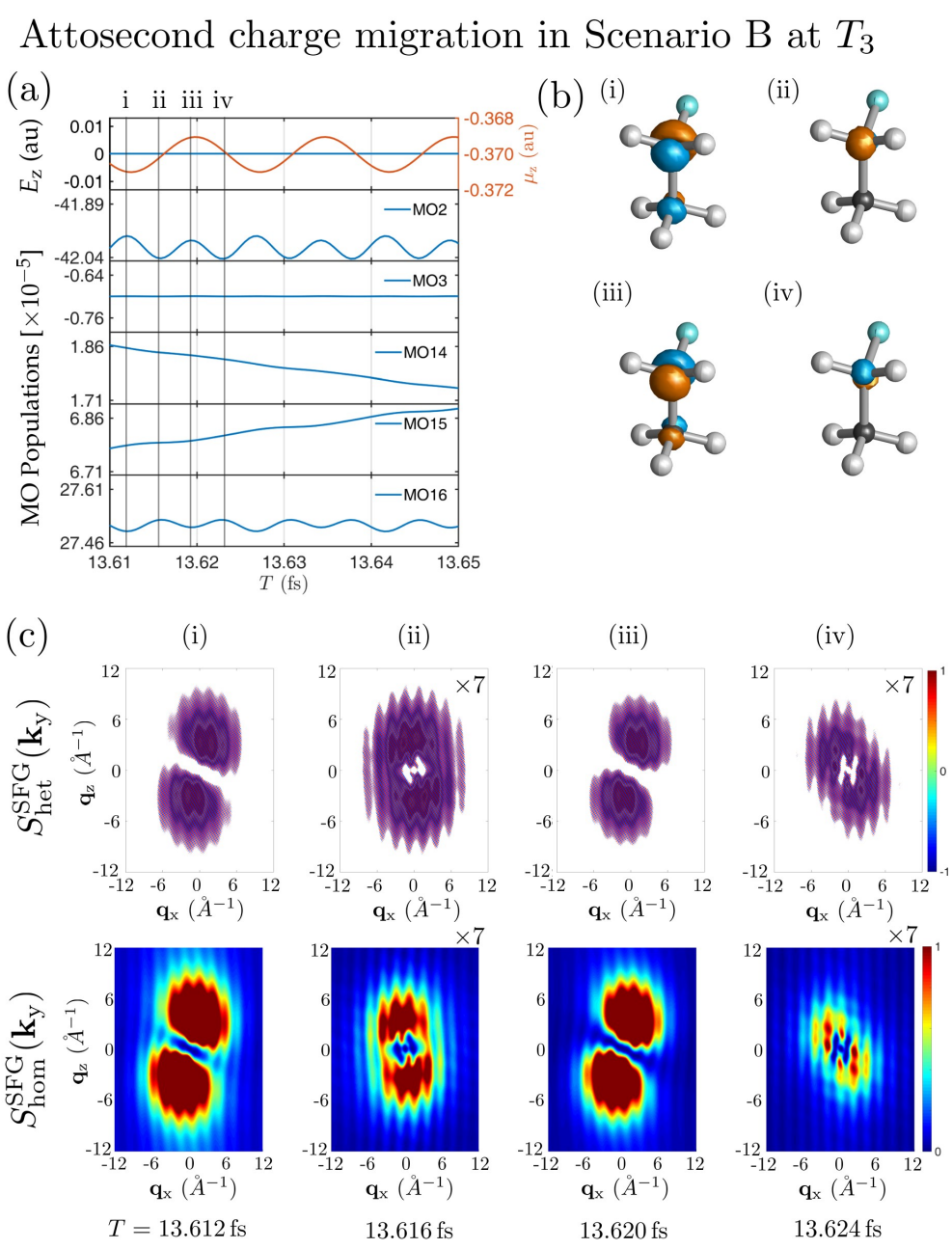


Figure S9: Same as Figure S4 but for Scenario B at $T_3$.

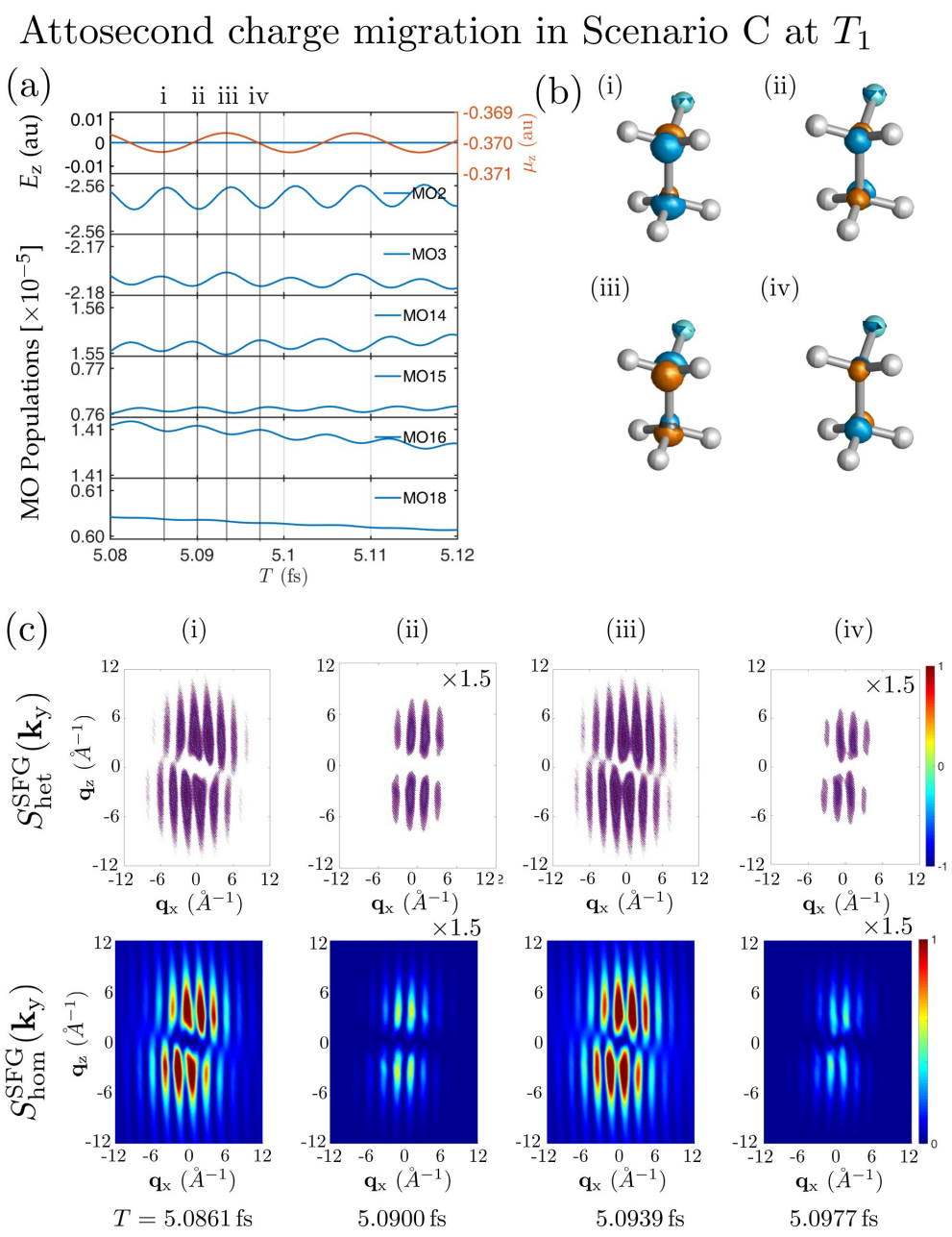


Figure S10: Same as Figure S4 but for Scenario C at $T_1$.

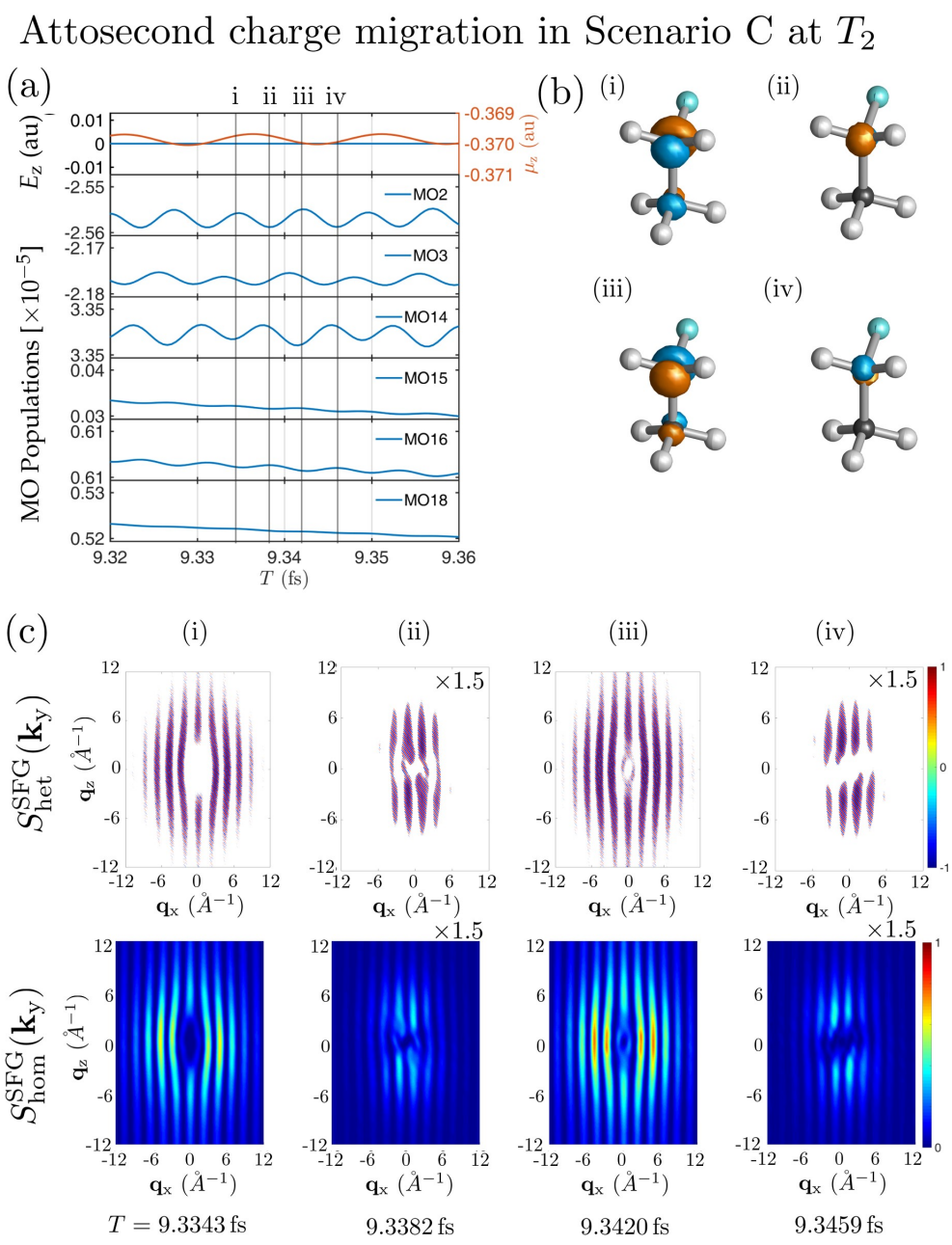


Figure S11: Same as Figure S4 but for Scenario C at $T_2$.

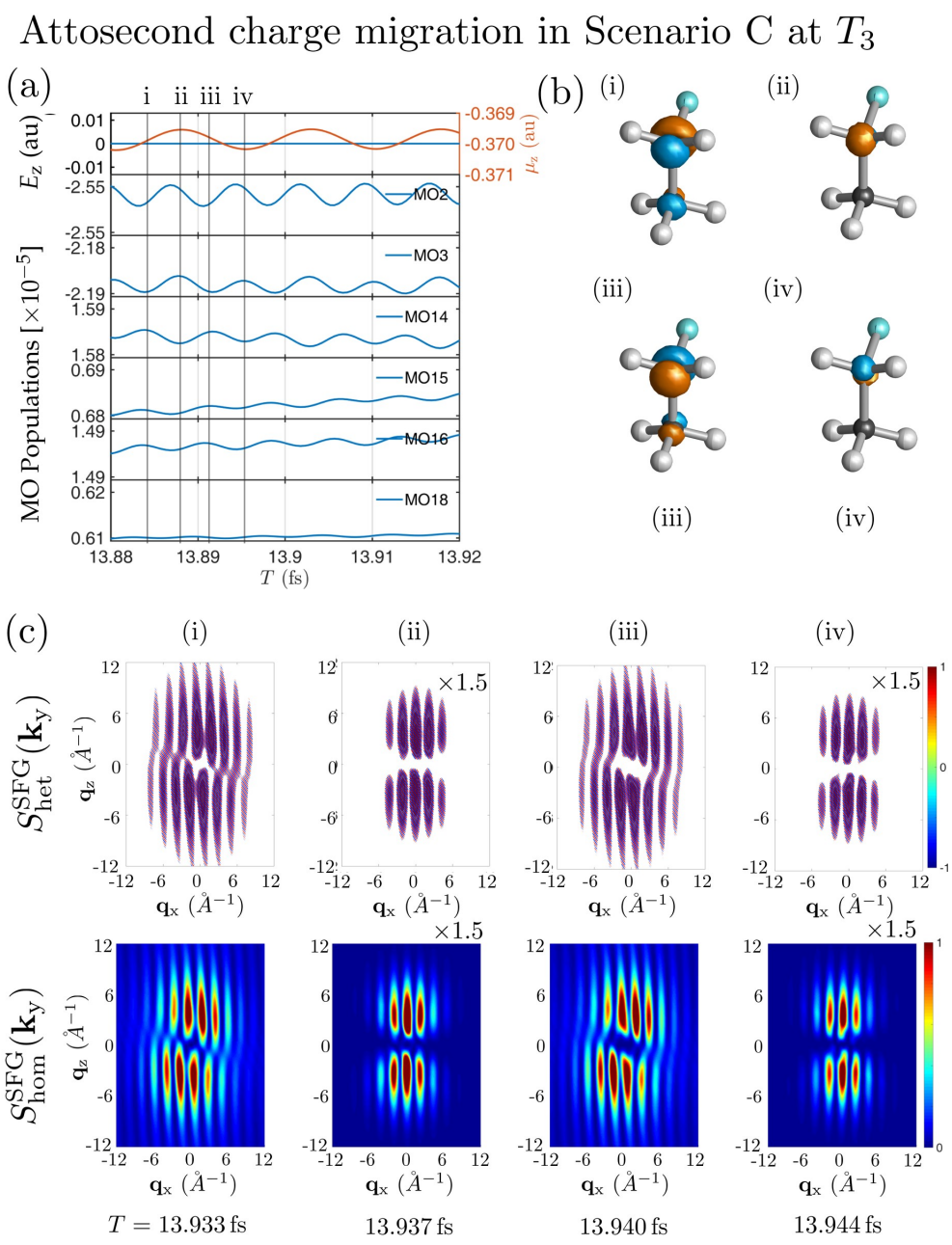


Figure S12: Same as Figure S4 but for Scenario C at $T_3$.

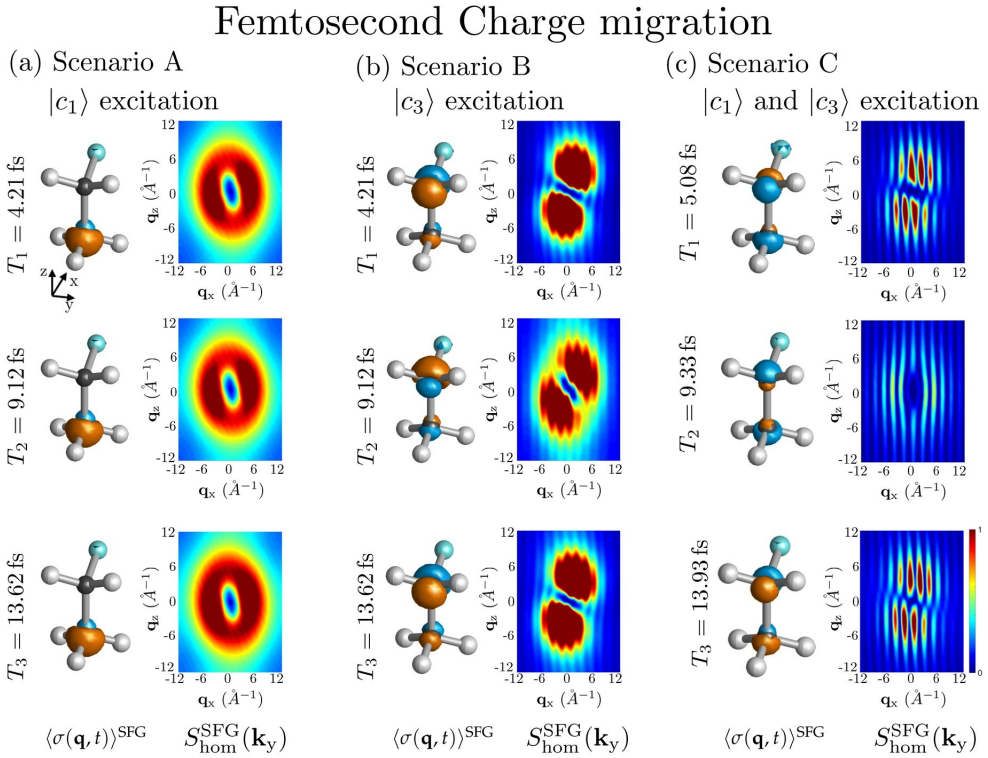


Figure S13: Charge migration following the (a) scenario A; $|c_1\rangle$ excitation, (b) scenario B; $|c_3\rangle$ excitation, and (c) scenario C; $|c_1\rangle$–$|c_3\rangle$ excitations and the corresponding homodyne diffraction signals.

# S3 Effect of the Phase Cycling Protocol

## Scenario A, $|c_1\rangle$ excitation

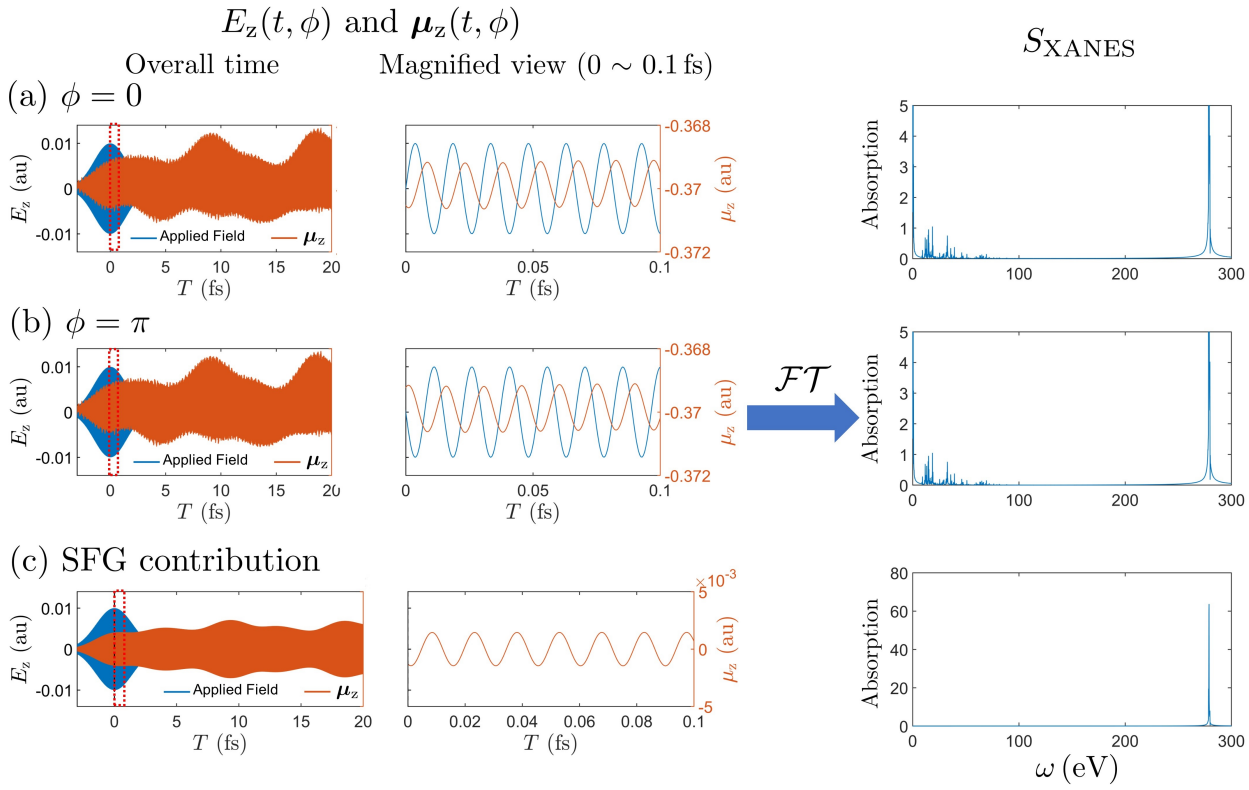


Figure S14: RT-TDDFT simulation of the $E_z(t,\phi)$, $\boldsymbol{\mu}_z(t,\phi)$, and the corresponding absorption spectrum under field phase (a) $\phi = 0$, (b) $\phi = \pi$, and (c) the SFG contribution obtained by eq. 2.9 following the Scenario A.

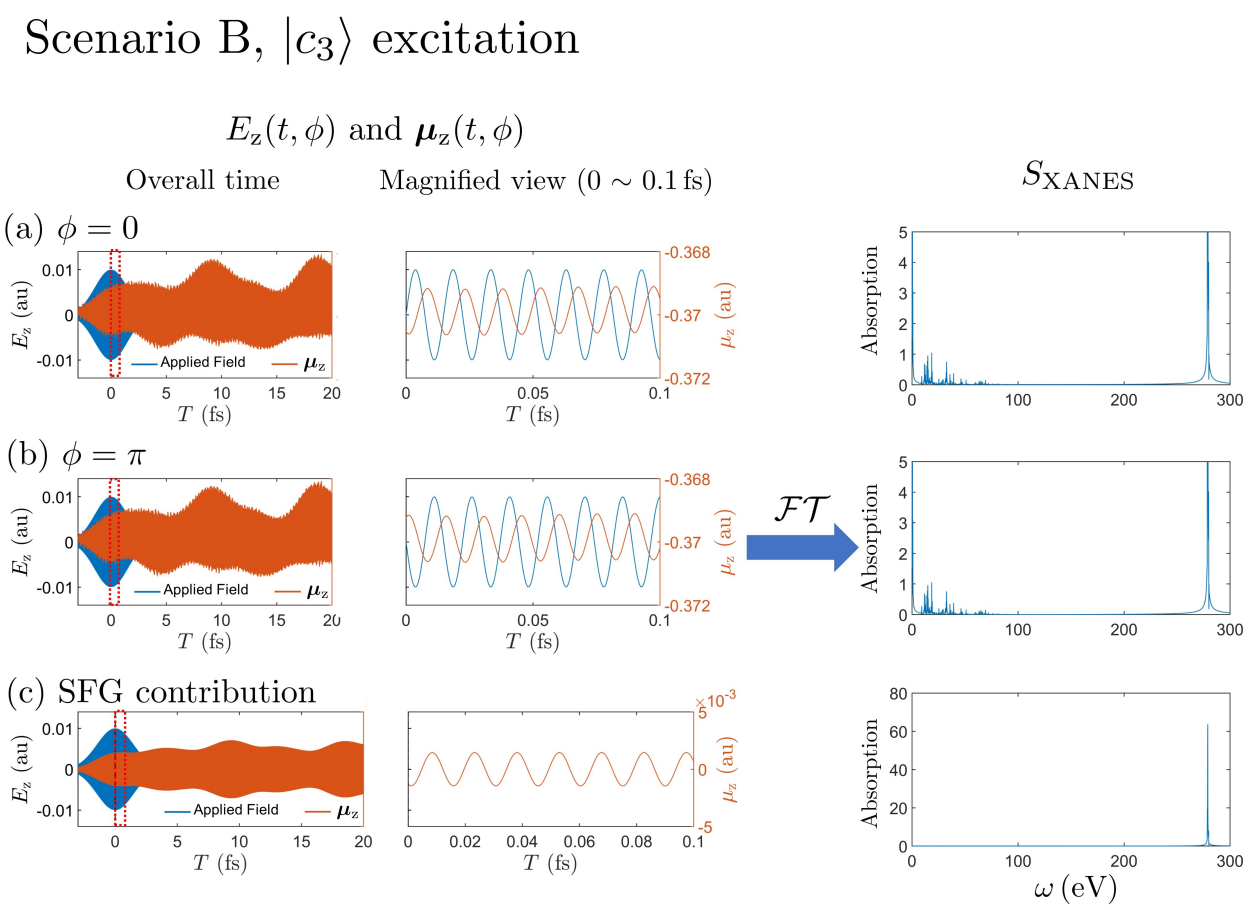


Figure S15: Same as Figure S14 but for Scenario B.

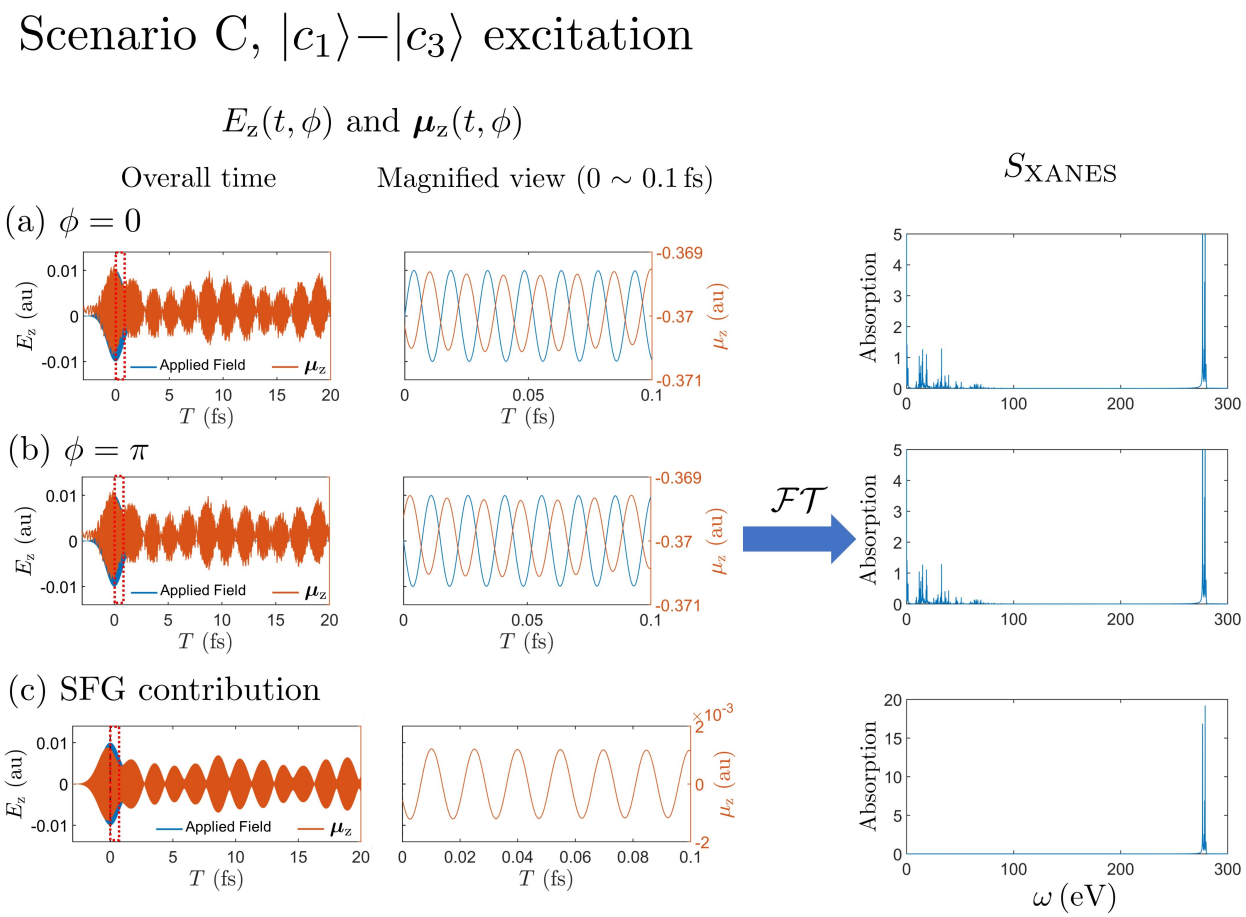


Figure S16: Same as Figure S14 but for Scenario C.